Received: 16 July 2017 | Revised: 21 August 2017 | Accepted: 4 September 2017

DOI: 10.1111/ajt.14503

ORIGINAL ARTICLE

AJT

Defining a microRNA-mRNA interaction map for calcineurin inhibitor induced nephrotoxicity

Christopher J. Benway[1,2] | **John Iacomini**[1,2,3,4]

[1]Department of Integrative Physiology and Pathobiology, Tufts University School of Medicine, Boston, MA, USA

[2]Graduate Program in Genetics, Sackler School of Graduate Biomedical Sciences, Tufts University School of Medicine, Boston, MA, USA

[3]Graduate Program in Immunology, Sackler School of Graduate Biomedical Sciences, Tufts University School of Medicine, Boston, MA, USA

[4]Tufts University School of Medicine, Boston, MA, USA

Correspondence
John Iacomini
Email: john.iacomini@tufts.edu

Calcineurin inhibitors induce nephrotoxicity through poorly understood mechanisms thereby limiting their use in transplantation and other diseases. Here we define a microRNA (miRNA)-messenger RNA (mRNA) interaction map that facilitates exploration into the role of miRNAs in cyclosporine-induced nephrotoxicity (CIN) and the gene pathways they regulate. Using photoactivatable ribonucleoside-enhanced crosslinking and immunoprecipitation (PAR-CLIP), we isolated RNAs associated with Argonaute 2 in the RNA-induced silencing complex (RISC) of cyclosporine A (CsA) treated and control human proximal tubule cells and identified mRNAs undergoing active targeting by miRNAs. CsA causes specific changes in miRNAs and mRNAs associated with RISC, thereby altering post-transcriptional regulation of gene expression. Pathway enrichment analysis identified canonical pathways regulated by miRNAs specifically following CsA treatment. RNA-seq performed on total RNA indicated that only a fraction of total miRNAs and mRNAs are actively targeted in the RISC, indicating that PAR-CLIP more accurately defines meaningful targeting interactions. Our data also revealed a role for miRNAs in calcineurin-independent regulation of JNK and p38 MAPKs caused by targeting of *MAP3K1*. Together, our data provide a novel resource and unique insights into molecular pathways regulated by miRNAs in CIN. The gene pathways and miRNAs defined may represent novel targets to reduce calcineurin induced nephrotoxicity.

KEYWORDS

basic (laboratory) research/science, genomics, immunosuppression/immune modulation, kidney failure/injury, molecular biology: micro RNA, molecular biology: mRNA/mRNA expression, translational research/science

1 | INTRODUCTION

Calcineurin inhibitors are a cornerstone of immunosuppression for transplant patients and have dramatically reduced rejection rates because of their ability to prevent T cell activation.[1] This ability has also led to their use in the treatment of autoimmune diseases.[2,3] However, short- or long-term use of calcineurin inhibitors such as CsA and tacrolimus is associated with nephrotoxicity.[1,4] Calcineurin inhibitor induced nephrotoxicity (CIN) can be acute or chronic.[5] While acute CIN is reversible following drug withdrawal, chronic CIN is irreversible causing glomerular and vascular disease, abnormal tubular function, and increased blood pressure.[6] Acute and chronic CIN can only be diagnosed by invasive renal biopsy, usually after significant kidney damage has occurred. There a significant gap in our knowledge in the diagnosis, prevention and treatment of CIN driven by an incomplete understanding of its molecular basis. While CIN appears to result from processes that cause apoptosis of renal tubular cells, generation of reactive oxygen species, and epithelial-mesenchymal transition (EMT),[7-9] how these processes are regulated is not completely understood. Developing an understanding of the gene pathways involved in CIN

and how they are regulated could offer novel prevention and treatment strategies to reduce toxicity allowing better usage of these potent immunosuppressive drugs.

MicroRNAs (miRNAs) are a class of small, noncoding RNAs that post-transcriptionally regulate the expression of more than 60% of protein coding genes in humans[10-16] and control cellular function in several disease processes.[17-29] We previously demonstrated that miRNAs play an important role in controlling acute renal injury resulting from ischemia and reperfusion.[30] It is now apparent that the miRNAs play a key role in regulating many aspects of renal injury.[31-45] Because miRNAs regulate gene expression, understanding how their expression is altered throughout the progression of a disease lends itself to the discovery of new pathways involved in disease progression, development of phenotyping assays and biomarkers, and identification of novel therapeutic targets. We hypothesized that identification of genes undergoing active targeting by miRNAs would allow us to identify pathways altered due to CIN and define global changes in gene regulation that contribute to disease and potential novel targets for therapeutic intervention. To test our hypothesis, we used crosslinking and immunoprecipitation (CLIP) methodology to identify miRNAs and mRNAs associated with Argonaute 2 (AGO2) protein in the RNA-induced silencing complex of CsA treated and control human proximal tubule cells and then used that information to define a miRNA-mRNA targetome for CIN. This analysis revealed several pathways under regulation by miRNAs in CsA treated cells and an unexpected role for miRNAs in regulating expression of MAPKs.

2 | MATERIALS AND METHODS

2.1 | Cell culture

HK-2 cells (ATCC, Manassas, VA) were cultured in serum-free keratinocyte medium (Thermo Fisher, Waltham, MA) supplemented with Epidermal Growth Factor 1-53 and Bovine Pituitary Extract and treated with 5 μg/mL CsA (Sigma-Aldrich, St. Louis, MO) or ethanol as a vehicle control as previously described.[46]

2.2 | Animal model of CsA nephrotoxicity

Ten- to 12-week-old male C57BL/6J mice were purchased from The Jackson Laboratory (Bar Harbor, ME) and housed under microisolator conditions. All experiments were performed with approval of our Institutional IACUC. CsA nephrotoxicity was induced as previously described.[46-48]

2.3 | RNA-Seq

HK-2 cells were treated for 48 hours with CsA (5 μg/mL) or vehicle control (0.1% ethanol). Four replicates were used for each condition. Polyadenylated mRNAs were isolated and used to generate multiplexed cDNA libraries for Illumina sequencing.

2.4 | AGO2-PAR-CLIP

PAR-CLIP was performed as previously described.[49,50]

2.5 | PAR-CLIP bioinformatic analysis and ingenuity pathway analysis

Details are provided in Supplemental Materials and Methods.

2.6 | Western blot assay

Cell cultures were lysed in RIPA buffer supplemented with phosphatase and protease inhibitors. SDS-PAGE was performed using 4-12% Novex NuPage Bis-Tris gels in MOPS buffer under reducing conditions (Thermo Fisher). Monoclonal antibodies used for were anti-MAP3K1/MEKK1 (Clone 2F6, Novus Biologicals, Littleton, CO) and anti-GAPDH (Clone 71.1, Sigma-Aldrich).

2.7 | Real-time quantitative PCR

PCR was performed as previously described[46] after preparing cDNA using the High Capacity cDNA Reverse Transcription Kit (Applied Biosystems, Foster City, CA). TATA-binding protein (human *TBP* or mouse *Tbp*) mRNA was used as normalization control. Relative quantification was calculated using the ΔΔCT method and assays were performed in triplicate or quadruplicate.[51]

2.8 | Availability of data and material

All raw sequencing data and associated processed PAR-CLIP, RNA-seq, and miRNA-seq datasets discussed in this publication have been deposited in NCBI's Gene Expression Omnibus and are accessible through GEO Series accession number GSE98670.

3 | RESULTS

3.1 | PAR-CLIP defines miRNAs associated with the RISC complex in human proximal tubule cells treated with CsA

We performed AGO2-PAR-CLIP on human kidney proximal tubule cells (HK-2 cells) treated with CsA or vehicle as a control. HK-2 cells were cultured in medium supplemented with 100 μM 4-thiouracil (4-SU) and then treated with CsA. The cells were then exposed to UV light (365 nm) to crosslink RNAs to associated RNA binding proteins. AGO2-associated RNAs (miRNAs and mRNAs) were then isolated by immunoprecipitation using AGO2-specific antibodies (Figure S1). AGO2-associated RNAs were then purified, reverse transcribed, amplified, and made into cDNA libraries and sequenced. PAR-CLIP was performed in duplicate for each experimental condition and the resulting Illumina sequencing reads were pooled for maximal read depth. Raw sequencing clusters, trimmed reads and mapped reads are

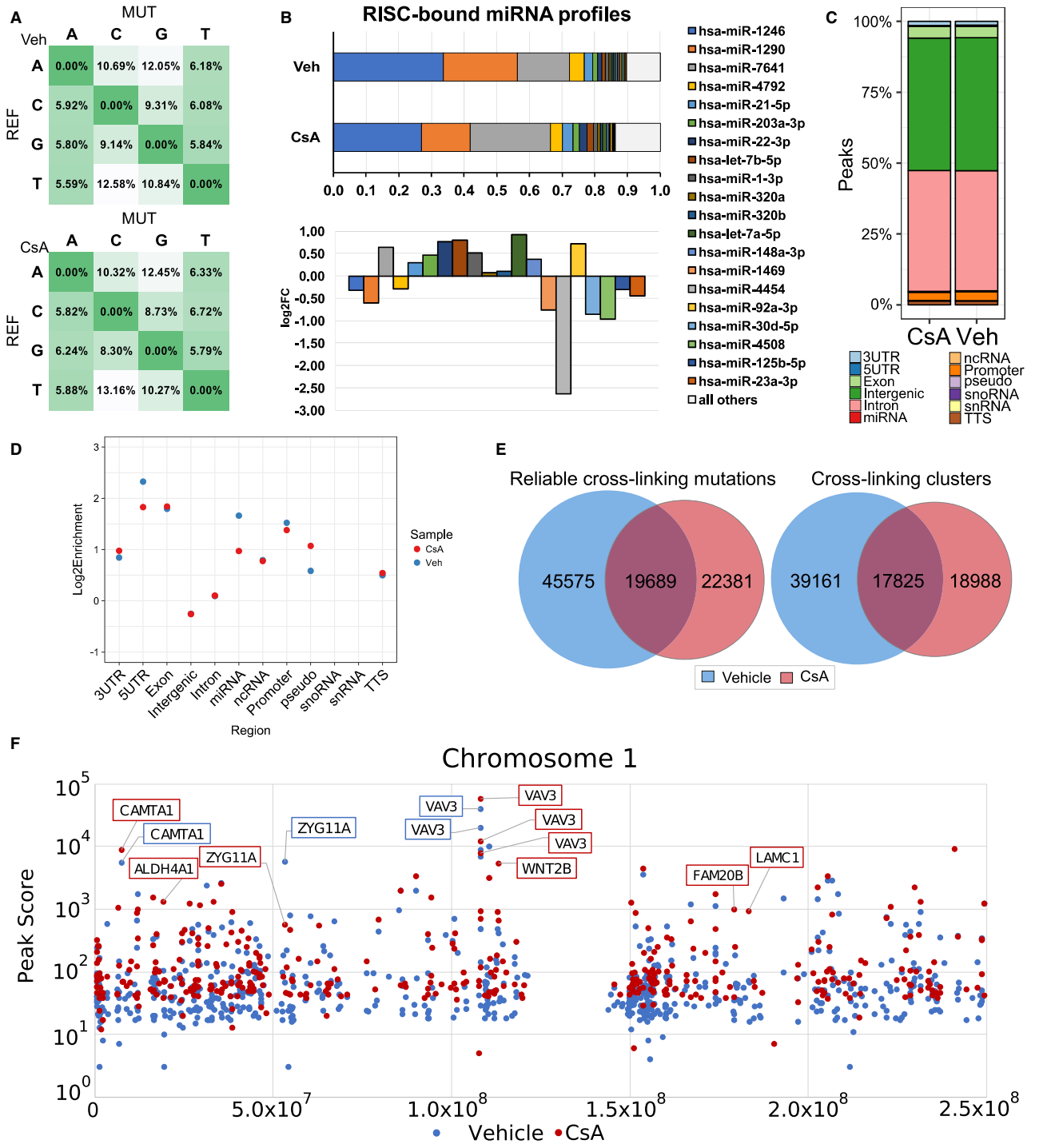

FIGURE 1 Analysis of RISC-bound RNAs and miRNAs and mRNAs obtained by AGO2-PAR-CLIP in CsA-treated HK-2 cells. (A) Mutational frequencies of all possible transitions in AGO2-PAR-CLIP sequences derived from vehicle (Veh) and CsA-treated HK-2 cells. (B) Proportions of the top 20 miRNAs that were detected in AGO-PAR-CLIP libraries by alignment to miRNAbase v21 reference database. Below, log2 fold change of top 20 miRNAs detected in RISC complex after treatment with CsA. (C) Genomic distribution of crosslinking sites identified by AGO2-PAR-CLIP in vehicle and CsA-treated HK-2 cells. (D) Log2 enrichment of AGO2 crosslinking sites in genomic regions based on normalization to relative region sizes in the reference genome. 3UTR: 3' untranslated region, 5UTR: 5' untranslated region, ncRNA: non-coding RNA, snoRNA: small nucleolar RNA, snRNA: small nuclear RNA, TTS: transcription termination site. (E) Venn diagrams demonstrating the number of unique and shared AGO2 crosslinking mutations and sequence clusters in vehicle vs CsA-treated HK-2 cells. Reliable crosslinking mutations are determined by fitting a binomial distribution to assess the significance of T > C mutations. Mutations with an FDR (Benjamini-Hochberg method) less than 0.05 are considered "reliable." For crosslinking sequence clusters, a zero-truncated negative binomial regression is first used to identify enriched clusters of overlapping sequences. The enriched clusters (with FDR < 0.05) that also contain a reliable mutation are considered "crosslinking clusters." (F) PIPE-CLIP peak scores of AGO2 crosslinking sites in vehicle (blue) and CsA-treated (red) HK-2 cells mapping to chromosome 1 (excluding intergenic and intronic regions)

shown in Figure S2. Incorporation of 4-SU into nascent RNAs leads to crosslinking to RNA binding proteins (RBPs) following exposure to UV light. RNAs that are crosslinked exhibit T to C transitions when subsequently reverse transcribed into cDNAs. The frequency of reads containing crosslinking T to C or A to G (negative strand) mutations was higher than all other mutations indicating enrichment for RNAs actively targeted in the RISC (Figure 1A).

We mapped the AGO2-PAR-CLIP sequence reads obtained to the miRNAbase v21 reference pre-miRNA hairpin sequences. Mapping and subsequent quantification were performed with miRNADeep2, allowing for one mutation.[52] Initial results revealed an abundance of three mature microRNAs (hsa-miR-1246, hsa-miR-1290, and hsa-miR-7641) accounting for nearly 70% of all normalized expression in both samples (Figure 1B, Table S1).

TABLE 1 Differential expression of top mature miRNAs increased and decreased in RNA-induced silencing complex after cyclosporine A treatment

miRNA	Veh_seq(norm)	CsA_seq(norm)	FoldChange	Log2FC
hsa-miR-10a-5p	7	2801	396.71	8.63
hsa-miR-98-5p	14	451	31.91	5.00
hsa-miR-424-5p	35	630	17.83	4.16
hsa-miR-574-3p	57	776	13.74	3.78
hsa-miR-378a-3p	438	4581	10.46	3.39
hsa-miR-184	85	863	10.18	3.35
hsa-miR-5684	71	673	9.53	3.25
hsa-miR-744-5p	71	668	9.45	3.24
hsa-miR-7975	57	527	9.32	3.22
hsa-miR-103a-3p	71	646	9.15	3.19
hsa-miR-107	71	646	9.15	3.19
hsa-miR-17-5p	71	592	8.38	3.07
hsa-miR-101-3p	325	2481	7.64	2.93
hsa-miR-27a-5p	169	1162	6.85	2.78
hsa-miR-99a-5p	304	1992	6.56	2.71
hsa-let-7c-5p	388	2133	5.49	2.46
hsa-miR-3687	78	413	5.31	2.41
hsa-miR-499a-5p	120	630	5.24	2.39
hsa-miR-486-5p	169	885	5.22	2.38
hsa-miR-34a-5p	120	613	5.11	2.35
hsa-miR-4508	3100	1466	0.47	−1.08
hsa-miR-199a-5p	600	282	0.47	−1.09
hsa-miR-199a-3p	1335	597	0.45	−1.16
hsa-miR-199b-3p	1335	597	0.45	−1.16
hsa-let-7d-5p	14	5	0.38	−1.38
hsa-miR-542-5p	14	5	0.38	−1.38
hsa-miR-7847-3p	14	5	0.38	−1.38
hsa-miR-130a-3p	1766	586	0.33	−1.59
hsa-miR-30c-5p	1843	608	0.33	−1.60
hsa-miR-200c-3p	2232	581	0.26	−1.94
hsa-miR-6802-5p	21	5	0.26	−1.96
hsa-miR-4485-3p	1194	261	0.22	−2.20
hsa-miR-3168	247	49	0.2	−2.34
hsa-miR-4454	3686	548	0.15	−2.75
hsa-miR-22-5p	42	5	0.13	−2.96
hsa-let-7e-5p	148	16	0.11	−3.19
hsa-miR-5100	78	5	0.07	−3.84
hsa-miR-6773-5p	367	22	0.06	−4.08
hsa-miR-4787-5p	318	16	0.05	−4.29
hsa-miR-4516	996	11	0.01	−6.52

Reads mapping to hsa-miR-1246 and hsa-miR-1290 may represent other non-coding RNA reads because nearly all such reads contained a mismatch to the reference hsa-miR-1290 hairpin which aligned to the U2 small nuclear RNA RNU2 perfectly (Figure S3), consistent with other reports.[53] Similarly, hsa-miR-7641 has been identified as a derivative of rRNA repeats within 5S ribosomal pseudogene 387.[54] We therefore excluded these miRNAs from analysis. Based on normalized read counts we then ranked up and down-regulated miRNAs relative to control samples following CsA treatment (Table 1). Hsa-miR-10a-5p exhibited the greatest increase in RISC binding after CsA treatment, whereas hsa-miR-4516 was decreased most. Many miRNAs (n = 118) were also identified that were present only in vehicle or CsA samples (Table S1).

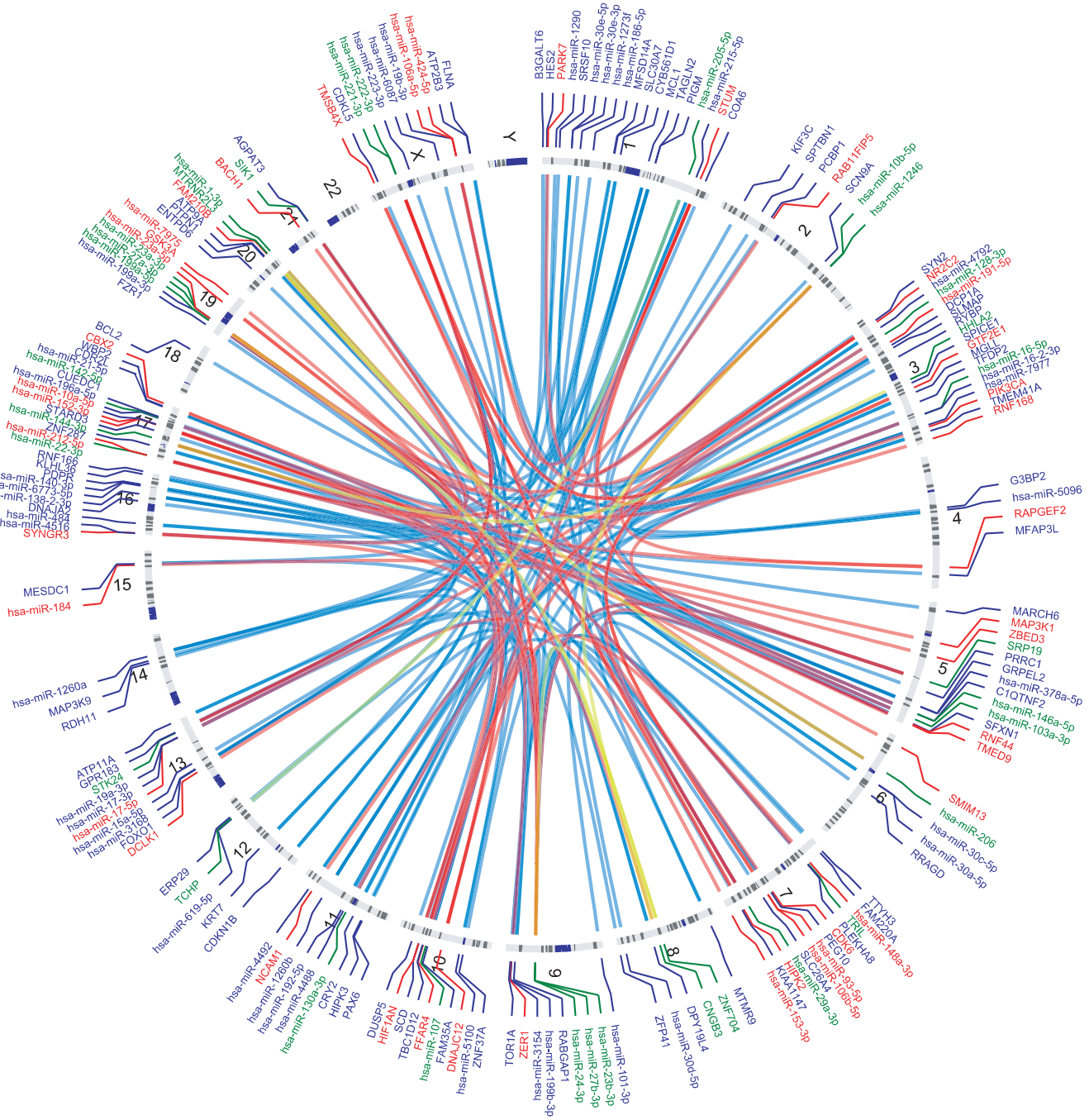

FIGURE 2 The miRNA targetome induced by CsA treatment of HK-2 cells is genome wide. Genome-wide differential targeting of mRNAs by miRNAs in CsA (red) treated HK-2 cells compared to vehicle control (blue). Arcs link target genes containing seed complementarity in the 3'UTR to immunoprecipitated miRNAs (positions 2-8) with their putative miRNA regulator, as determined by AGO2-PAR-CLIP. Green arcs represent common miRNA-mRNA interactions between sample groups. Genes and miRNA genes in green text were observed in both CsA and vehicle control but may reflect sample-specific targeting interactions

3.2 | miRNA-binding events in the RISC complex of human proximal tubule cells treated with CsA

PIPE-CLIP identifies clusters of overlapping sequences by computing counts of sequences overlapping by at least one nucleotide and then determines reliable crosslinking to RNA binding proteins based on induced T > C mutations. This makes it possible to estimate the degree to which sequences throughout the genome are undergoing targeting in association with AGO2. We identified 56 985 and 36 812 significant crosslinking sites in sequence clusters from vehicle and CsA-treated libraries respectively (Tables S2 and S3). Within these clusters, we observed 65 263 and 42 069 reliable T > C mutations. Annotation of the sequences in each cluster revealed that many map to intergenic and intronic regions of the genome (Figure 1C). However, normalization to the relative sizes of the genomic regions revealed enrichment for crosslinking sites in 3'UTR, exon, and 5'UTR transcript regions as well as promoter and transcription termination sites (Figure 1D, Table S4).

We next compared crosslinking mutations in sequence clusters using PIPE-CLIP in CsA and vehicle control libraries. We identified 45 575 sequences with reliable cross-linked mutations that were unique to vehicle controls, 19 689 in both CsA treated and vehicle controls, and 22 381 unique to CsA treated samples (Figure 1E). These sequences were present in 39 161 clusters from vehicle control, 17 825 from both CsA treated and vehicle controls, and 18 988 from CsA treated samples (Figure 1E). PIPE-CLIP peak scores were computed for all clusters based on read counts of sequences containing mutations. Strength and location of binding based on depth of read coverage and number of mutations varied between CsA and vehicle-treated samples (Figure 1F). Many crosslinking sites were present in both vehicle and control samples of which many exhibited significant increases or decreases in peak signal strength after CsA treatment.

3.3 | mRNAs in the AGO2 complex contain seed sequences of miRNAs identified by PAR-CLIP

Crosslinking sites based on mutations located within mRNAs accounted for 3264 and 2157 of total sites mapping to the 5' and 3' UTR and coding regions of sequences from vehicle and CsA-treated samples respectively (Table S4), representing a 3-fold enrichment when normalized to genomic region size. We assigned crosslinking miRNA clusters to mRNA targets by mapping them to the transcript crosslinking sites based on complementarity to the seed sequences from miRNA clusters we identified for each condition (Tables S5 and S6). Seed sequences that matched canonical 8-mer, 7-mer, and 6-mer seed sequences corresponding to miRNA positions 1-8, 1-7, 2-8, 1-6, 2-7, and 3-8 were analyzed. Since the major mechanism by which miRNAs regulate expression involves targeting the 3'UTR of mRNAs, we focused on clusters in this region of encoding genes.[55] Sixty-eight percent (514/748) of 3'UTR clusters in vehicle controls and forty-eight percent (257/530) of 3'UTR clusters in CsA treated samples contained a canonical seed match for at least one of the miRNAs we identified by PAR-CLIP.

Mapping of canonical 7-mer seed matches indicated that miRNA-mRNA interactions in vehicle and CsA-treated samples occur throughout the genome (Figure 2). miRNA-mRNA interactions unique to either vehicle or CsA-treated samples are also apparent (Figure 2). The 10 miRNAs with most the frequent seed matches in vehicle and CsA-treated samples are shown in Table 2. Five out of the top 10 miRNAs were present in both vehicle and CsA treated samples, while five seed matches were present only in either vehicle or CsA treated samples (Table 2). However, only 21.29% (23/108) and 31.08% (23/74) of the mRNAs predicted to be targeted by miRNAs in vehicle and CsA treated samples respectively were present in both samples. Thus, although several mRNAs containing miRNA seed sequences were abundant in both conditions, relatively few targeting interactions were shared.

3.4 | Comparison of PAR-CLIP and RNA-seq

To examine the extent to which changes in total miRNA and mRNA expression reflect the changes observed in the RISC by PAR-CLIP we examined miRNA expression profiles using miRNA-seq on total RNA from HK-2 cells after treatment with CsA or vehicle control (Figure S4, Tables S7 & S8). Of the 2586 mature miRNAs in miRNAbase v21, 1575 were detected at any level (Figure S5A). The top 100 expressed miRNAs accounted for 98.8% of reads across all samples (Figure S5B). Differential expression analysis identified that 72 miRNAs were differentially regulated after CsA treatment (Benjamini-Hochberg adjusted P value < .1), of which 35 were up-regulated and 37 were down-regulated when compared with control samples (Figure 3A). We next compared sequencing data obtained from miRNA-seq and PAR-CLIP. miRNA-seq identified 1542 mature miRNAs in vehicle samples and 1525 in CsA-treated samples. Of these miRNAs, 177 in vehicle and 124 in CsA treated samples were also identified by PAR-CLIP while 26 mature miRNAs in vehicle and 13 in CsA treated samples were uniquely identified by PAR-CLIP (Figure 3B).

We next examined the fraction of cellular mRNAs undergo active targeting following CsA treatment by performing RNA-seq on HK-2 cells treated with CsA or vehicle as a control. Differential expression analysis identified 7688 genes that were differentially expressed in CsA treated samples with an FDR-adjusted P-value less than .05 (Benjamini-Hochberg method). Of these differentially expressed genes, 1625 exhibited an absolute log2 fold-change greater than 1, 160 exhibited an absolute log2 fold-change greater than 2, and 35 exhibited an absolute log2 fold-change greater than 3 (Figure 4A). Comparing RNA-seq and PAR-CLIP sequencing data revealed that 868 mRNA clusters in CsA treated samples and 1503 in vehicle controls identified by PAR-CLIP were also observed by RNA-seq, while 775 were shared in all data sets (Figure 4B). PAR-CLIP identified 68 and 286 mRNA clusters that were uniquely present in CsA or vehicle samples (Figure 4B). Fifty-nine clusters identified by PAR-CLIP were present in both CsA and vehicle controls (Figure 4B).

TABLE 2 Top miRNA seed matches in 3'UTR

Sample	miRNA	Targets	Genes
Veh	hsa-miR-1260a/b	28	*CBFA2T3, CCBE1, CCL22, CCNB1, CRY2, CUX2, CYB561D1, DCX, FUT11, HSPA12A, IRX6, KCNE3, KIF5A, LUC7L, MGLL, NFATC2, NRXN1, PAX8, PCBP1, PRKN, RAB34, SESN2, SMARCD1, TLX3, TMEM119, WBP2, ZNF37A, ZNF426*
Veh	hsa-miR-7977	27	*ADAR, ATP9A, C2CD4B, C8orf33, CCNI2, CDKL5, DHRS7B, FAM127B, FUT11, G3BP2, GATAD2A, GNE, IFI44L, MARCH1, NRXN1, PCBP1, PTPN18, RAB34, SESN3, SLC16A3, TCN2, TLE3, TMED9, TNF, WSB1, ZNF37A, ZNF704*
Veh	hsa-miR-5100	24	*AGTR2, C14orf180, CD164, CLDN10, CUEDC1, DSG1, EXPH5, GUCY1A2, KCNN3, PAG1, PLCG2, QDPR, RBFOX2, RIMKLA, SCD, SLC22A18AS, SMIM12, SPICE1, SZT2, TALDO1, TBC1D16, TSC1, TUFT1*
Veh	hsa-miR-103a-3p/107	23	*AGRN, ANXA8L1, BRWD1, C12orf73, CAMK2A, CHMP1B, DCP1A, FLYWCH1, G3BP2, KLF13, KLHL36, LDOC1, NDUFB4, PCBP1, PDE6A, PPARD, PXDN, SAT2, STAT5B, TOR1A, TRIAP1, USP22, XRN1*
Veh	hsa-miR-140-3p	23	*BACE1, CLDND1, DCAF7, DDAH1, DIP2C, DYRK2, FFAR4, KDSR, KIAA1147, METRNL, PDK3, PHACTR2, PXDN, RAB34, RXRA, SLMAP, SMIM12, TAGLN2, TBC1D12, TUSC2, ZC3H12D, ZFP41, ZRANB1*
Veh	hsa-miR-199a-5p	22	*AAK1, C2CD4B, CMPK2, COL2A1, DNAL4, FRRS1L, GATAD2B, GOPC, HES2, KIF3C, PTPN18, SAT2, SESN2, SESN3, SIRPG, SLC35B4, SLC7A1, STARD3, TMED9, TMOD2, TRIL, WSB1*
Veh	hsa-miR-30e-3p	21	*AASS, ABCB5, BAHCC1, C12orf73, CD164, CDKN2B, CLDN10, CSPG4, DESI1, DNAJC8, FRRS1L, GATAD2B, GRIK4, NR2F1, PLEKHA8, PPP1R12B, RBFOX2, SLC7A11, SNX9, TTC8, ZNF655*
Veh	hsa-miR-23a/b-3p	20	*AASS, CCDC50, DNAJC8, EAF1, EHD2, FOXO1, HNRNPR, KDM3B, LAMC1, PACSIN1, PEG10, PLCG2, PPP1CB, SH3BP2, SRP19, STX1B, TMEM74B, TRIM66, ZNF544, ZNF704*
Veh	hsa-miR-27a/b-3p	20	*AASS, DHX33, DPY19L4, FOXO1, GRAMD3, MAU2, MCL1, MESDC1, PHACTR2, PRDM10, RABGAP1, RAX, SCN9A, SRP19, STARD7, STX1B, TECRL, TLCD2, TRAF3IP1, TUFT1*
Veh	hsa-miR-5096	20	*AASS, ABCB5, AGPAT3, CHIC1, DESI1, DPY19L4, EXPH5, MCL1, PROX2, PXDN, RORA, RYBP, SMIM7, SMU1, SNX9, TMPO, TMSB4X, TTC8, TUFT1, ZBTB47*
CsA	hsa-miR-27a/b-3p	18	*AMOTL2, ATP6V1A, CBX2, CCNJ, CELF1, DNAJC12, FFAR4, MAP3K1, MAU2, PHACTR2, PKIA, PRDM10, RUNX1, SIK1, SPEN, SRP19, TSC22D3, ZBTB34*
CsA	hsa-miR-140-3p	17	*ARPC4, ARSB, C15orf53, CCNJ, COX10, DDAH1, FFAR4, HES7, KIAA1147, L2HGDH, PHACTR2, PPP1R15B, RAB34, RXRA, TSC22D3, ZFAND5, ZRANB1*
Csa	hsa-miR-144-3p	16	*ANGPT1, CYSTM1, DNAJC12, FAM127A, HHLA2, KPNA2, MAP3K1, POLR3K, PTGFRN, RAB34, SESN3, SLC4A8, SRP19, TMEM117, TMSB4X, TSC22D3*
CsA	hsa-miR-199a-5p	15	*CMPK2, CNGA3, DNAL4, FRRS1L, GATAD2B, GPR26, HSPA5, MYO1D, SEC61A1, SESN3, SH2B3, SLC7A1, TBC1D13, THBD, TRIL*
CsA	hsa-miR-128-3p	15	*AMOTL2, CCNJ, CXCL3, DNAJC12, FFAR4, GAD1, MAP3K1, MAU2, MYO1D, PHACTR2, RUNX1, SIK1, SPEN, TSC22D3, ZBTB34*
CsA	hsa-miR-205-5p	14	*BRWD1, CHIC1, FOXE3, GALNT13, HDX, KIAA1147, NCOA2, PKD1L2, SLC30A9, SMU1, TCHP, TMED9, WDR17, ZNF544*
CsA	hsa-miR-101-3p	13	*ANGPT1, CYSTM1, DNAJC12, HHLA2, KPNA2, LCN10, MAP3K1, PTGFRN, SLC4A8, SRP19, TMEM117, TMSB4X, TSC22D3*
CsA	hsa-miR-103a-3p/107	12	*BRWD1, LOC101928841, NDUFB4, PPARD, RDH10, RHOQ, RUNX1, SLC7A5, STUM, TSC22D3, ZBTB34, ZFAND5*
Csa	hsa-miR-23a/b-3p	11	*BTBD10, CBX2, DNAJC12, EHD2, LAMC1, NPAP1, SRP19, SYNGR3, TMED10, ZNF585B, ZNF704*
CsA	hsa-miR-125b-5p	10	*ABCC5, CD81, CYP26B1, NR3C2, PEG10, PHLDB1, RAB11FIP5, RNF44, TMEM201, YRDC*

3.5 | Gene pathways regulated by miRNAs following CsA treatment

Using Ingenuity Pathway Analysis (IPA) on the sets of transcripts identified by AGO2-PAR-CLIP, we identified the canonical pathways enriched in gene sets composed of all mRNA targets in either vehicle (n = 3264) or CsA (n = 2157) treated samples (Figure 5A,B). Of the top 20 canonical pathways enriched in each group, 11 were enriched in both (Figure S6). Thus, despite only modest overlap in the transcripts that are targeted by miRNAs in both conditions, several critical pathways are found to be regulated by the RISC complex in CsA-treated and vehicle control HK-2 cells related to cell-cell adhesion, integrin-cytoskeleton signaling, and calcium signaling. We also identified the pathways enriched only in the set of genes identified by PAR-CLIP that were also downregulated after CsA treatment as determined by RNA-seq (Figure 5C and Figure S6). To determine the function

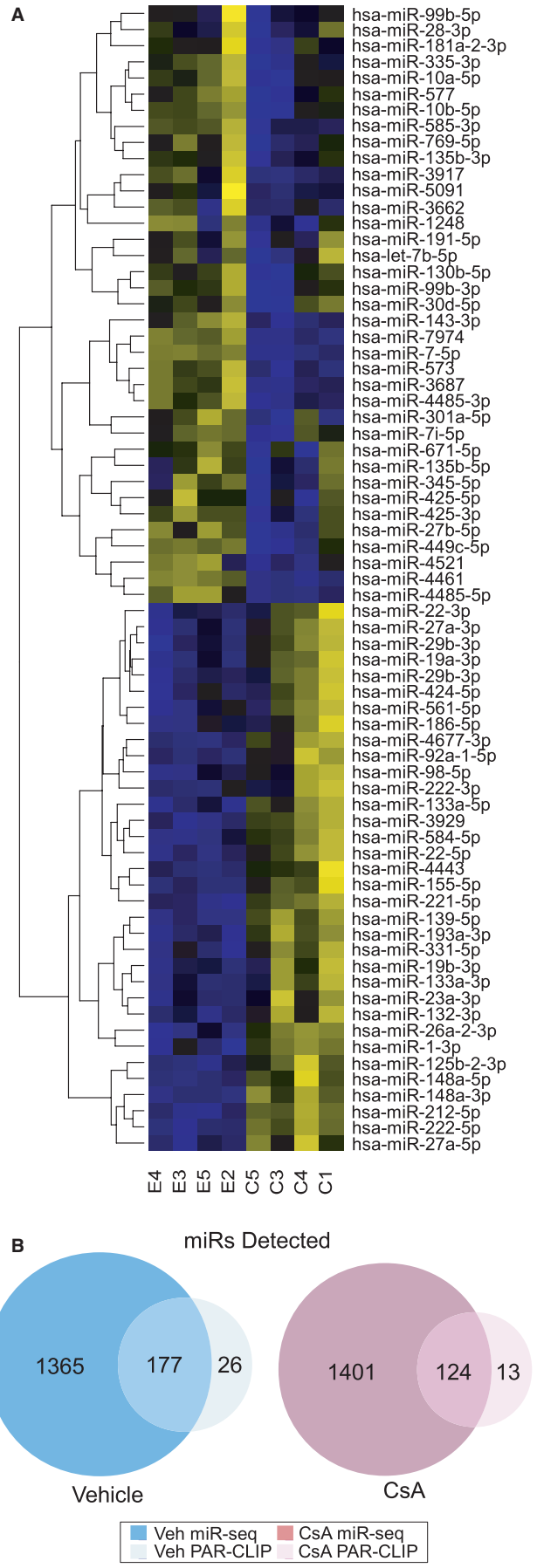

FIGURE 3 Differential expression of miRNAs by RNA-seq after cyclosporine treatment of HK-2 cells. (A) Heat map depicting normalized miRNA expression in CsA-treated samples, C, or ethanol-treated vehicle control samples, E. Heat map represents the 72 differentially expressed miRNAs after CsA treatment as determined by analysis by DESeq2 (Benjamini-Hochberg adjusted P value < .1; yellow = up-regulation, blue = down-regulation). (B) Proportion of miRNAs identified in AGO2-PAR-CLIP (light blue, light pink) that were also detected by miRNA-seq in vehicle (dark blue) and CsA-treated (violet) HK-2 cells

of the most abundant miRNAs targeting high confidence binding sites, we analyzed the transcripts which were previously matched in the 3'UTR with the most frequently occurring miRNA seeds by IPA. In vehicle treated HK-2 cells the top enriched canonical pathways were PPAR Signaling and PXR/RXR activation. In CsA-treated cells the top enriched canonical pathways were VDR/RXR Activation and Glucocorticoid Receptor Signaling. Notably, the Glucocorticoid Receptor Signaling pathway was also identified as one of the top canonical pathways enriched in CsA-treated PAR-CLIP transcripts and exhibited the highest enrichment in transcripts that were exclusively regulated by miRNAs in CsA-treated cells (Figure S7). The miRNA-targeted transcripts in CsA-treated proximal tubule cells involved in Glucocorticoid Receptor Signaling are C-X-C motif chemokine ligand 3 (*CXCL3*), heat shock protein family A (Hsp70) member 5 (*HSPA5*), mitogen-activated protein kinase kinase kinase 1 (*MAP3K1*), nuclear receptor coactivator 2 (*NCOA2*), nuclear receptor subfamily 3 group C member 2 (*NR3C2*), and TSC22 domain family member 2 (*TSC22D2*).

To determine the putative roles of miRNA-mRNA targeting relationships we integrated RNA-seq expression data of the target genes and related pathway members and implemented the Ingenuity Molecule Activity Predictor to model downstream effects (Figure 5D). In Glucocorticoid Receptor Signaling there is crosstalk between the active glucocorticoid receptor complex and MAPK signaling, including direct binding to JNK which mediates inhibition of the JNK pathway and trans-repression of AP-1.[56] 3'UTR targeting of *MAP3K1/MEKK1* and *TSC22D3/GILZ* was identified by PAR-CLIP in CsA-treated HK-2 cells. In RNA-seq, a corresponding decrease in expression was found in both genes (*MAP3K1/MEKK1* = −1.12 log2FC, adj *P*-value = 1.80×10^{-23}; *TSC22D3/GILZ* = −0.61 log2FC, adj *P*-value = 7.65×10^{-35}). Further, in both genes, the PAR-CLIP target clusters contained seed sequences complementary to miR-27a-3p and miR-101-3p, miRNAs which were up regulated after CsA treatment (+0.384 log2FC, FDR = 0.007; +0.259 log2FC, FDR = 0.25, respectively). Down-regulation of these transcripts is predicted to inhibit JNK and p38 signaling and allow activation of ERK1/2 (Figure 5D). In Jurkat T cells, CsA inhibits JNK and p38 but not ERK pathways.[57] In our RNA-seq data, we observed down-regulation of *MAPK10/JNK3* −1.69 log2FC, adj P-value = 2.24×10^{-12}). *HSPA5* and *NR3C2*, the mineralcorticoid receptor, were both detected by PAR-CLIP in CsA-treated HK-2 cells and both transcripts are significantly up-regulated compared to vehicle control (+1.48 log2FC, adj P-value = 6.21×10^{-157} and +1.29 log2FC, adj *P*-value = 1.23×10^{-21}; Figure 5D). Increased expression of both genes contributes to reduced signaling by the glucocorticoid-GCR

dimer complex, thus suggesting that JNK/p38 inhibition may occur upstream.[58,59]

3.6 | miR-101-3p targets *MAP3K1* transcripts in vitro

Based on the identification of RISC binding to the 3'UTR of *MAP3K1* exclusively in CsA-treated HK-2 cells, we hypothesized that miRNA targeting of *MAP3K1* might contribute to CsA-dependent down regulation of *MAP3K1* and thus inhibition of p38 and JNK signaling. The cluster sequence identified by AGO2-PAR-CLIP in the 3'UTR of *MAP3K1* contains seed complementarity to miRNAs which were also identified in CsA treated AGO2-PAR-CLIP samples. Hsa-miR-144-3p matched the cluster with 7mer canonical seed complementarity, whereas hsa-miRNA-101-3p and hsa-miRNA-27a-3p matched the cluster with canonical 6mer and offset-6mer seed complementarity, respectively (Figure 6A). Seed complementarity was also found for hsa-miRNA-128-3p, hsa-miRNA-199b-3p, and hsa-miRNA-223-3p (not shown). As previously mentioned, hsa-miR-101-3p and hsa-miR-27a-3p were up-regulated in CsA-treated HK-2 cells. Further, in our analysis of the RISC-bound miRNAs, hsa-miRNA-101-3p was enriched 7.64-fold in CsA treated samples (Table 2). In contrast, expression of *MAP3K1* was decreased after 48 hours by RNA-seq (−1.12 log2 fold change, adjusted P-value = 1.76×10^{-46}, Figure 6B). We confirmed the CsA-induced down regulation of *MAP3K1* mRNA by qPCR (Figure 6C).

To test whether miRNA-101-3p targets the 3'UTR of *MAP3K1*, we examined whether miRNA-101-3p could regulate *MAP3K1* by expressing miR-101 using a lentiviral vector. Compared to empty vector control (GFP only), expression of the pre-miR-101 hairpin in HK-2 cells reduced expression of MAP3K1 protein (Figure 6D, E). In HK-2 cells, we detected two MAP3K1 bands at ~140 kDa and ~55 kDa. Full length MAP3K1 has been found to regulate cell migration and pro-survival signaling whereas the caspase-3-generated cleavage product promotes apoptosis.[60] Both MAP3K1 fragments, were decreased in cells transfected with the pre-miRNA-101 expression vector. To determine whether MAP3K1 down regulation in HK-2 cells was related to calcineurin inhibitor nephrotoxicity in vivo, we examined expression of transcripts in whole kidney samples of mice administered CsA (30 mg/kg/day) or olive oil control as previously described.[46] Compared to control mice, CsA-treated mice exhibited decreased levels of *MAP3K1* mRNA after 2 and 3 weeks of daily injections (Figure 6F).

4 | DISCUSSION

Our primary goals were to define the physiologically relevant miRNA-targeting interactions that may contribute to the molecular pathology of calcineurin inhibitor nephrotoxicity and more completely define the effect of CsA on proximal tubule gene expression. While previous studies have sought to achieve a similar goal,[46,61] they relied on approaches with significant limitations.[62,63] We therefore sought to define the transcriptome-wide miRNA targetome in proximal tubule cells to understand how miRNAs regulate renal injury resulting from CsA treatment. We used PAR-CLIP, a technique that achieves high-resolution mapping of RBPs and active miRNA-mRNA targeting interactions by defining RNAs intimately associated with RISC complex protein AGO2. Comparing RNA-seq and PAR-CLIP data revealed that while 868 mRNA clusters in CsA-treated samples and 1503 in vehicle controls identified by PAR-CLIP were also observed by RNA-seq, PAR-CLIP identified 68 and 286 mRNA clusters that were uniquely present in CsA or vehicle samples. We conclude that changes in total

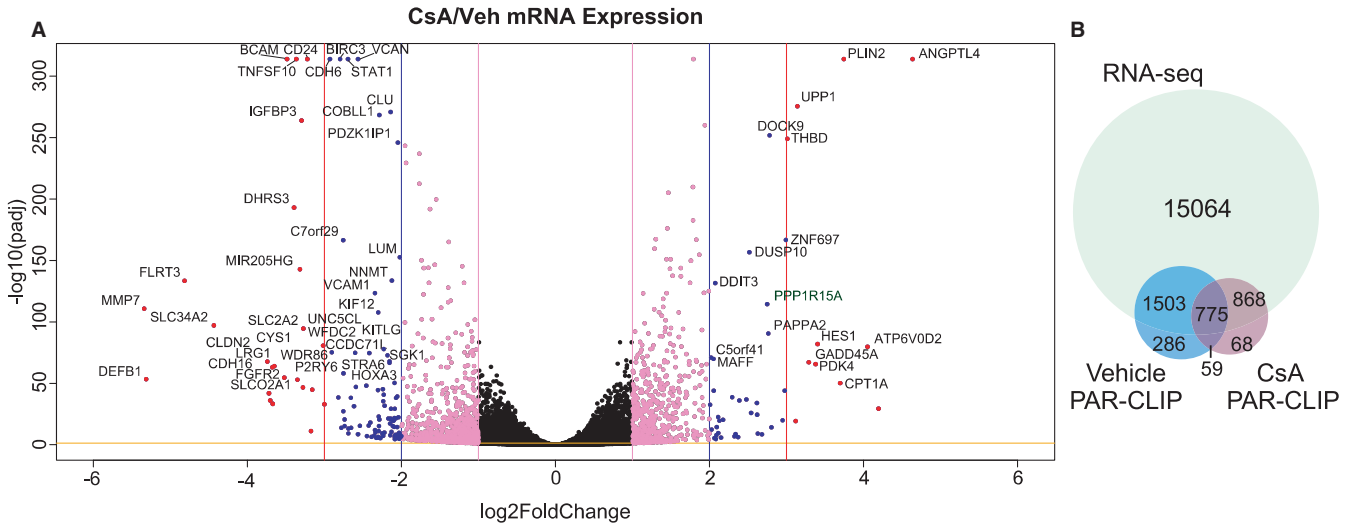

FIGURE 4 Differential expression of transcripts after CsA treatment of HK-2 cell. Poly-A enriched RNA-seq was performed on HK-2 cells treated with or vehicle control. (A) Volcano plot shows differential expression of all genes after cyclosporine treatment. Adjusted P-value of .05 is indicated by horizontal orange line. Coloring of points depicts log2FC > [1] (pink), >[2] (blue), and >[3] (red). Gene symbols are displayed on genes for which log2FC > [2] and -log10(padj) > 50. (B) Proportion of all mRNAs detected by RNA-seq (light green) that were also identified by AGO2-PAR-CLIP of vehicle (blue) and CsA-treated (violet) HK-2 cells

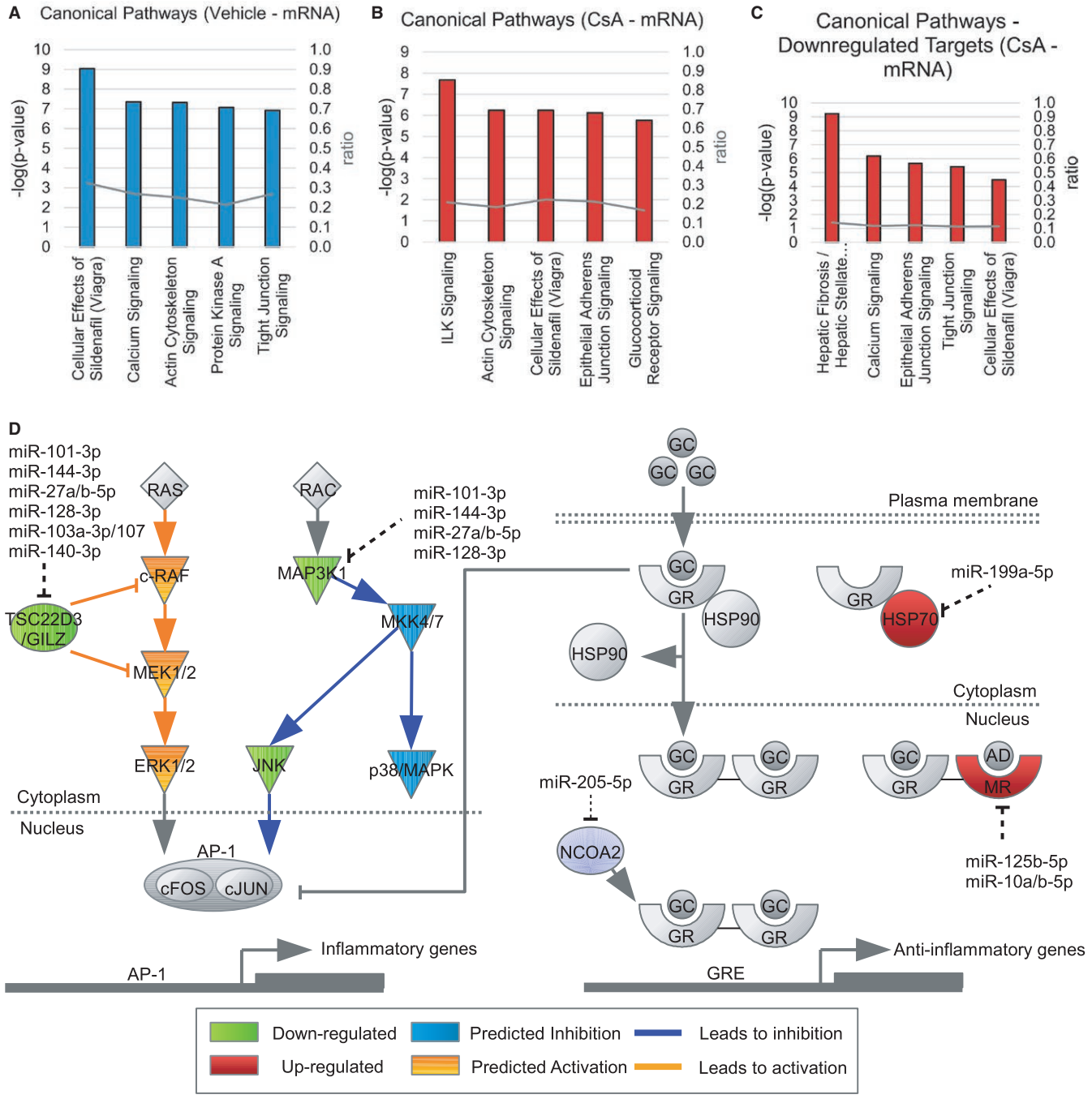

FIGURE 5 Ingenuity Pathway Analysis of canonical pathways targeted by miRNAs in CsA and vehicle-treated HK-2 cells. Bar graphs indicate the top five canonical pathways enriched in the mRNA targets of miRNAs as identified by AGO2-PAR-CLIP in (A) vehicle and (B) CsA-treated HK-2 cells. Bars represent the negative log of P-value and lines represent the total fraction of the canonical gene set matched. (C) Bar graph indicates the top five canonical pathways enriched in CsA-treated AGO2-PAR-CLIP mRNA targets that were also down-regulated in RNA-seq after CsA treatment. (D) Diagram of the glucocorticoid receptor signaling pathway which cross talks with MAPK-ERK, MAPK-JNK, and MAPK-p38 signaling. The pathway is integrated with RNA-seq differential expression data from CsA-treated HK-2 cells and predictive downstream analysis conducted with Ingenuity Pathway Analysis. Left, putative RISC target sites were identified by AGO2-PAR-CLIP in the 3'UTRs of TSC22D3/GILZ and MAP3K1, which inhibit MAPK-ERK and activate MAPK-JNK and MAPK-p38 signaling, respectively. The putative miRNA regulators shown share seed sequence homology. Genes that are shaded green (TSC22D3/GILZ, MAP3K1/MEKK1, JNK3) were down regulated in CsA-treated HK-2 cells in the RNA-seq experiment. Genes that are shaded orange (c-RAF, MEK1/2, ERK1/2) are predicted to be activated because of TSC22D3/GILZ down regulation. Genes that are shaded in blue (MKK4/7, p38/MAPK) are predicted to be inhibited because of MAP3K1 down regulation. Right, putative RISC target sites were identified by AGO2-PAR-CLIP in the 3'UTRs of HSPA5/HSP70 and NR3C2/MR that can both reduced signaling by the glucocorticoid-GCR dimer complex, as well as the transcriptional activator NCOA2. Genes that are shaded red (HSPA5/HSP70 and NR3C2/MR) were up regulated in CsA-treated HK-2 cells in the RNA-seq experiment. Expression of NCOA2 was unchanged

cellular miRNA abundance alone cannot predict functional targeting of mRNAs.

We found that a unique set of miRNAs is enriched in the RISC complex of HK-2 cells and that this RISC-enriched profile is altered after treatment with CsA. This suggests that differential targeting is a fundamental mechanism for regulating the CsA-induced gene program in these cells. Importantly, changes in total miRNA abundance after CsA treatment defined by RNA-seq of total cellular RNA did not correlate with increased or decreased miRNA RISC binding. Thus, only a fraction of expressed miRNAs actively target mRNAs. This phenomenon has been observed previously in an AGO-PAR-CLIP study of TP53-dependent miRNA-AGO2 association in which most miRNAs differentially expressed in the RISC associated with AGO2 did not correspond to relative abundance in total RNA samples.[64] While we do not know why only a relatively small number of total miRNAs are bound to AGO2, we speculate that some miRNAs may compete for binding to AGO2 better than others. While little is known about the rules of miRNAs binding to the targeting complex, AGO2 seems to be able to reshape the fundamental properties of RNA-RNA binding and allows oligonucleotides to bind more like RNA binding proteins with a high binding constant than typical RNA oligos.[65] We speculate that the ability of different miRNAs to associate with AGO2 and affect changes in binding may influence which miRNAs are represented in the RISC complex.

While control and CsA-treated cells exhibited expression of unique sets of miRNAs that were enriched in the targeting complex we did observe a relatively small degree of overlap. Only 21.29% (23/108) and 31.08% (23/74) of the mRNAs predicted to be targeted by the top 10 miRNAs in vehicle- and CsA-treated samples, respectively, were present in both samples. This suggests that under each condition each miRNA targets different gene sets. It is possible that this overlap may be related to the amount of time cells were exposed to CsA and that with a longer exposure this overlap will shrink. Nevertheless, it seems apparent that functional consequences of targeting are the result of a balance between differential expression of both miRNAs and mRNAs.

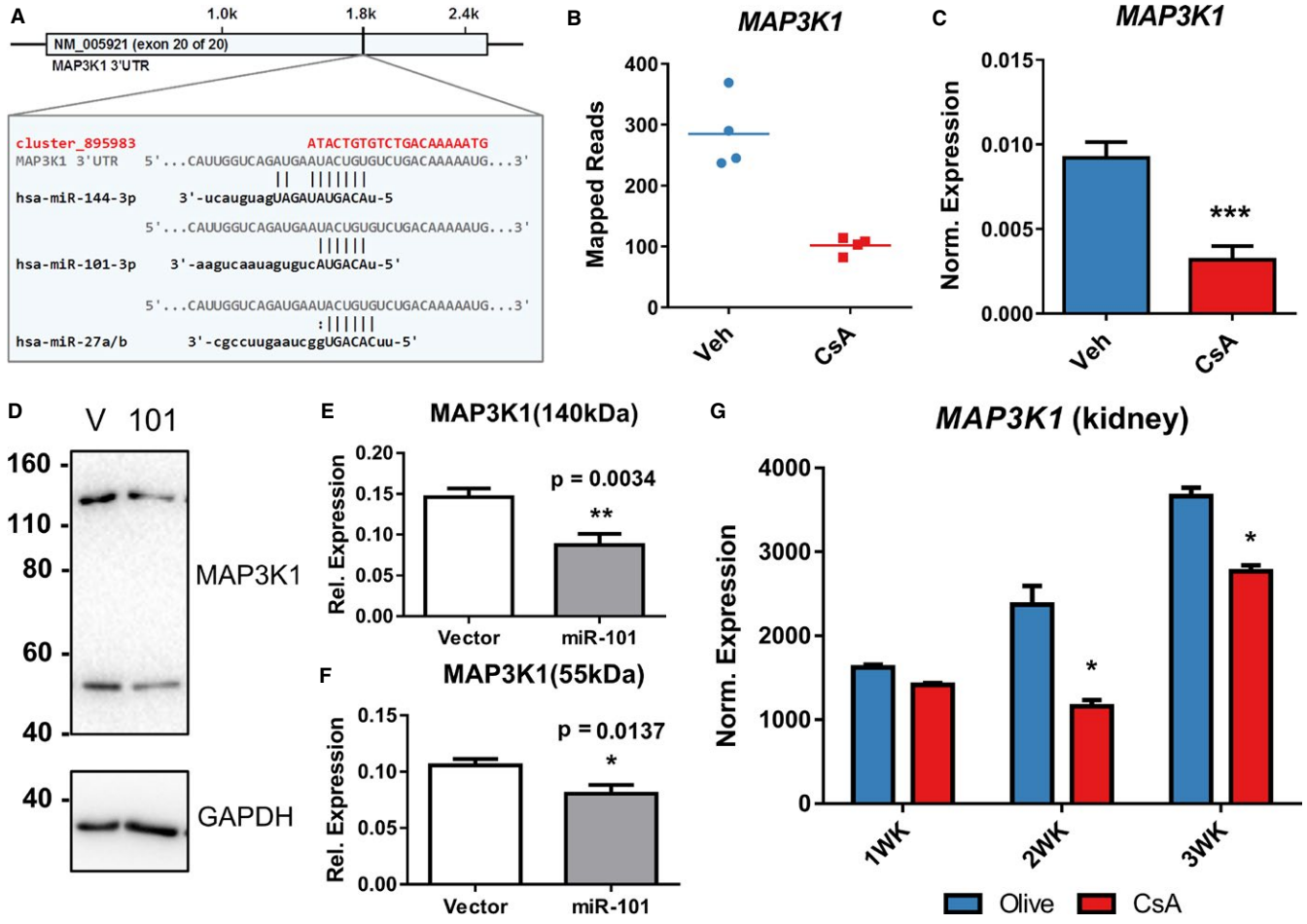

FIGURE 6 MiRNA-101-3p targets MAP3K1 expression in HK-2 cells. (A) AGO2-PAR-CLIP identified CsA-induced putative RISC binding in the 3'UTR of MAP3K1. Within the identified sequence cluster, 7mer and 6mer seed complementarity for miRNAs also immunoprecipitated by AGO2-PAR-CLIP are shown. (B) Raw mapped read counts in vehicle (Veh) and CsA-treated HK-2 cells mapping to the MAP3K1 gene from the RNA-seq experiment. (C) qPCR of MAP3K1 transcripts in HK-2 cells treated with CsA for 48 hours. (D) Immunoblot for MAP3K1 protein expression in HK-2 cells transfected with pLL3.7 lentiviral backbone expressing hsa-miRNA-101 or empty vector control, compared to GAPDH loading control. Representative of six replicate experiments. MAP3K1 immunoblot detects two bands at ~140 kDa and ~55 kDa. Quantification of 140kDa (E) and 55 kDa MAP3K1 (F) bands on Westerns normalized to GAPDH. (G) qPCR of MAP3K1 mRNA in whole kidney tissue from mice injected daily with CsA (30 mg/kg/day) or olive oil after 1, 2, and 3 weeks

Analysis of the AGO2-bound miRNA sequences by miRNAdeep2 suggested that three miRNAs (hsa-miR-1246, hsa-miR-1290, and hsa-miR-7641) were the most enriched in the RISC-complex and therefore the most active in targeting. However, hsa-miR-1246 and hsa-miR-1290 share perfect or near-perfect sequence homology with a processed fragment of the *RNU2* gene. In the PAR-CLIP reads assigned to hsa-miR-1290, 99.9% (26,158/26,185) contained an alignment mismatch. Most of these reads align perfectly to the *RNU2* gene. Further, no sequence reads aligning to hsa-miR-1290 were detected by miRNA-seq. Because mature hsa-miR-1246 shares perfect homology with the *RNU2* gene we cannot exclude the possibility that it is in fact present in the cells and in the RISC complex. Hsa-miR-7641 shares perfect homology with 5S ribosomal RNAs and it has been suggested that this miRNA is in fact derived from rRNA repeats. While, miR-7641 targeting of the cytokine CXCL1 in HUVEC cells has been suggested,[66] in our study, there was no evidence mature hsa-miR-7641 in miRNA-seq despite enrichment in the RISC complex.

PIPE-CLIP annotation of PAR-CLIP clusters allowed us to identify AGO2 crosslinking regions within 3'UTRs with a high degree of confidence. We coupled this information with IPA to identify pathways in which genes in the RISC complex play a role. Interestingly, 11 of the top 20 canonical pathways were enriched in CsA-treated samples and vehicle controls. While this may be related to the relatively short exposure to CsA in vitro, these data nevertheless suggest that miRNAs also play a central role in controlling several complex signaling pathways in control samples. CsA appears to influence tubular epithelial cells by affecting additional pathways such as the Intergrin Linked Kinase Signaling pathway which has been is known to play a major role in TGFβ induced EMT.[67] It also appears to affect Epithelial Adherent Junction Signaling which is critical for maintenance of E-cadherin junctions, which when disrupted drives EMT through effects on cytoskeleton reorganization, stress fiber formation, and cell adhesion.[68] Identification of these pathways that are central to EMT strongly suggests that our data reflect physiologically relevant regulation of processes occurring because of CIN that are regulated by the RISC complex.

CsA prevents T cell activation by inhibiting calcineurin, thereby affecting NFAT localization to the nucleus that is required for *IL-2* transcription. However, CsA has also been suggested to suppress activation of JNK and p38 upstream of mitogen activated protein kinase kinase kinases (MAPKK-Ks), preventing activation of *MAP3K1*, independently of its effect on calcineurin.[69] Our data revealed that clusters representing the 3'UTR of *MAP3K1/MEKK1* were present in the RISC of CsA-treated cells. Moreover, RNA-seq data showed a corresponding decrease in expression of these genes. The cluster sequence we identified in the 3'UTR of *MAP3K1* contained seed complementarity to several miRs identified in the RISC complex. Among these miRNAs, hsa-miR-101-3p and hsa-miR-27a-3p were up-regulated in CsA-treated HK-2 cells suggesting a possible targeting interaction. Importantly, miR-101-3p is also up-regulated 4.52-fold in the kidneys of mice treated with CsA,[70] indicating that up-regulation in HK-2 cells reflects changes observed in vivo. Expression of the pre-miR-101 hairpin in HK-2 cells resulted in reduced expression of *MAP3K1* protein, suggesting that miR-101 functionally targets *MAP3K1*. We suggest that CsA suppresses JNK and p38 by inducing targeting of *MAP3K1* by miR-101-3p. Thus, miR-101-3p plays a previously undiscovered role in regulating calcineurin independent effects of CsA.

Our results define a microRNA-mRNA targetome for calcineurin inhibitor induced nephrotoxicity. By identifying active targeting interactions that occur because of CsA treatment, we defined pathways that are likely to be affected and contribute to tissue injury. One major limitation of these experiments is the use of HK-2 cells. Clearly, HK-2 cells represent only a single cell type affected by CsA. We are currently conducting in vivo studies to determine how CsA alters miRNA expression and targeting of mRNAs in various cell types in the kidney. Nevertheless, this analysis provides novel insight into a miRNA mediated mechanism by which CsA affects calcineurin independent processes that could contribute to side effects by affecting cellular activation and or cell death. While the physiological role of the pathways, miRNAs and mRNAs we identified remain to be elucidated, these data serve as a novel resource for the community that could help lead to the identification of new druggable targets that could reduce toxicity associated with CsA.

ACKNOWLEDGMENTS

The authors wish to thank Thomas Tuschl and Marcus Hafner for kindly teaching us the art of PAR-CLIP, the Tufts University Sequencing Core Facility, and members of the Iacomini lab for helpful discussion. This work was supported in part by a Technology Access Grant awarded through Tufts University School of Medicine.

DISCLOSURE

The authors of this manuscript have no conflicts of interest to disclose as described by the *American Journal of Transplantation*.

REFERENCES

1. Bennett WM, DeMattos A, Meyer MM, Andoh T, Barry JM. Chronic cyclosporine nephropathy: the Achilles' heel of immunosuppressive therapy. *Kidney Int*. 1996;50(4):1089-1100.
2. Gipson DS, Trachtman H, Kaskel FJ, et al. Clinical trial of focal segmental glomerulosclerosis in children and young adults. *Kidney Int*. 2011;80(8):868-878.
3. Fernandes IC, Torres T, Selores M. Maintenance treatment of psoriasis with cyclosporine A: comparison between continuous and weekend therapy. *J Am Acad Dermatol*. 2013;68(2):341-342.
4. Ojo AO, Held PJ, Port FK, et al. Chronic renal failure after transplantation of a nonrenal organ. *N Engl J Med*. 2003;349(10):931-940.
5. Bobadilla NA, Gamba G. New insights into the pathophysiology of cyclosporine nephrotoxicity: a role of aldosterone. *Am J Physiol Renal Physiol*. 2007;293(1):F2-F9.
6. Chapman JR. Chronic calcineurin inhibitor nephrotoxicity-lest we forget. *Am J Transplant*. 2011;11(4):693-697.
7. Justo P, Lorz C, Sanz A, Egido J, Ortiz A. Intracellular mechanisms of cyclosporin A-induced tubular cell apoptosis. *J Am Soc Nephrol*. 2003;14(12):3072-3080.

8. Neria F, Castilla MA, Sanchez RF, et al. Inhibition of JAK2 protects renal endothelial and epithelial cells from oxidative stress and cyclosporin A toxicity. *Kidney Int*. 2009;75(2):227-234.
9. Slattery C, Campbell E, McMorrow T, Ryan MP. Cyclosporine A-induced renal fibrosis: a role for epithelial-mesenchymal transition. *Am J Pathol*. 2005;167(2):395-407.
10. Kim D, Sung YM, Park J, et al. General rules for functional microRNA targeting. *Nat Genet*. 2016;48(12):1517-1526.
11. Friedman RC, Farh KK, Burge CB, Bartel DP. Most mammalian mRNAs are conserved targets of microRNAs. *Genome Res*. 2009;19(1):92-105.
12. Friedman JM, Jones PA. MicroRNAs: critical mediators of differentiation, development and disease. *Swiss Med Wkly*. 2009;139(33–34):466-472.
13. Bartel DP. MicroRNAs: target recognition and regulatory functions. *Cell*. 2009;136(2):215-233.
14. John B, Enright AJ, Aravin A, Tuschl T, Sander C, Marks DS. Human MicroRNA targets. *PLoS Biol*. 2004;2(11):e363.
15. Lewis BP, Burge CB, Bartel DP. Conserved seed pairing, often flanked by adenosines, indicates that thousands of human genes are microRNA targets. *Cell*. 2005;120(1):15-20.
16. Huntzinger E, Izaurralde E. Gene silencing by microRNAs: contributions of translational repression and mRNA decay. *Nat Rev Genet*. 2011;12(2):99-110.
17. van Rooij E, Sutherland LB, Qi X, Richardson JA, Hill J, Olson EN. Control of stress-dependent cardiac growth and gene expression by a MicroRNA. *Science*. 2007;316(5824):575-579.
18. Hammond SM. MicroRNAs as oncogenes. *Curr Opin Genet Dev*. 2006;16(1):4-9.
19. Abe M, Akiyama T, Nakamura H, Kojima F, Harada S, Muraoka Y. First synthesis and determination of the absolute configuration of sulphostin, a novel inhibitor of dipeptidyl peptidase IV. *J Nat Prod*. 2004;67(6):999-1004.
20. Kim VN. Small RNAs: classification, biogenesis, and function. *Mol Cells*. 2005;19(1):1-15.
21. Kim VN. MicroRNA biogenesis: coordinated cropping and dicing. *Nat Rev Mol Cell Biol*. 2005;6(5):376-385.
22. Ambros V. The functions of animal microRNAs. *Nature*. 2004;431(7006):350-355.
23. Erson AE, Petty EM. MicroRNAs in development and disease. *Clin Genet*. 2008;74(4):296-306.
24. Calin GA, Liu CG, Sevignani C, et al. MicroRNA profiling reveals distinct signatures in B cell chronic lymphocytic leukemias. *Proc Natl Acad Sci USA*. 2004;101(32):11755-11760.
25. Calin GA, Ferracin M, Cimmino A, et al. A MicroRNA signature associated with prognosis and progression in chronic lymphocytic leukemia. *N Engl J Med*. 2005;353(17):1793-1801.
26. Lu J, Getz G, Miska EA, et al. MicroRNA expression profiles classify human cancers. *Nature*. 2005;435(7043):834-838.
27. Volinia S, Calin GA, Liu CG, et al. A microRNA expression signature of human solid tumors defines cancer gene targets. *Proc Natl Acad Sci USA*. 2006;103(7):2257-2261.
28. Melo SA, Kalluri R. miR-29b moulds the tumour microenvironment to repress metastasis. *Nat Cell Biol*. 2013;15(2):139-140.
29. Kasinski AL, Slack FJ. Epigenetics and genetics. MicroRNAs en route to the clinic: progress in validating and targeting microRNAs for cancer therapy. *Nat Rev Cancer*. 2011;11(12):849-864.
30. Godwin JG, Ge X, Stephan K, Jurisch A, Tullius SG, Iacomini J. Identification of a microRNA signature of renal ischemia reperfusion injury. *Proc Natl Acad Sci USA*. 2010;107(32):14339-14344.
31. Chandrasekaran K, Karolina DS, Sepramaniam S, et al. Role of microRNAs in kidney homeostasis and disease. *Kidney Int*. 2012;81(7):617-627.
32. Kantharidis P, Wang B, Carew RM, Lan HY. Diabetes complications: the microRNA perspective. *Diabetes*. 2011;60(7):1832-1837.
33. Chau BN, Xin C, Hartner J, et al. MicroRNA-21 promotes fibrosis of the kidney by silencing metabolic pathways. *Sci Transl Med*. 2012;4(121):121ra118
34. Xu X, Kriegel AJ, Liu Y, et al. Delayed ischemic preconditioning contributes to renal protection by upregulation of miR-21. *Kidney Int*. 2012;82(11):1167-1175.
35. Zarjou A, Yang S, Abraham E, Agarwal A, Liu G. Identification of a microRNA signature in renal fibrosis: role of miR-21. *Am J Physiol Renal Physiol*. 2011;301(4):F793-F801.
36. Zhong X, Chung AC, Chen HY, Meng XM, Lan HY. Smad3-mediated upregulation of miR-21 promotes renal fibrosis. *J Am Soc Nephrol*. 2011;22(9):1668-1681.
37. Moraes-Vieira PM, Bassi EJ, Larocca RA, et al. Leptin modulates allograft survival by favoring a Th2 and a regulatory immune profile. *Am J Transplant*. 2013;13(1):36-44.
38. Scian MJ, Maluf DG, Mas VR. MiRNAs in kidney transplantation: potential role as new biomarkers. *Expert Rev Mol Diagn*. 2013;13(1):93-104.
39. Dey N, Ghosh-Choudhury N, Kasinath BS, Choudhury GG. TGFbeta-stimulated microRNA-21 utilizes PTEN to orchestrate AKT/mTORC1 signaling for mesangial cell hypertrophy and matrix expansion. *PLoS ONE*. 2012;7(8):e42316.
40. Wang Q, Wang Y, Minto AW, et al. MicroRNA-377 is up-regulated and can lead to increased fibronectin production in diabetic nephropathy. *FASEB J*. 2008;22(12):4126-4135.
41. Kato M, Zhang J, Wang M, et al. MicroRNA-192 in diabetic kidney glomeruli and its function in TGF-β-induced collagen expression via inhibition of E-box repressors. *Proc Natl Acad Sci*. 2007;104(9):3432-3437.
42. Long J, Wang Y, Wang W, Chang BH, Danesh FR. MicroRNA-29c is a signature microRNA under high glucose conditions that targets Sprouty homolog 1, and its in vivo knockdown prevents progression of diabetic nephropathy. *J Biol Chem*. 2011;286(13):11837-11848.
43. Zhang Z, Peng H, Chen J, et al. MicroRNA-21 protects from mesangial cell proliferation induced by diabetic nephropathy in db/db mice. *FEBS Lett*. 2009;583(12):2009-2014.
44. Krupa A, Jenkins R, Luo DD, Lewis A, Phillips A, Fraser D. Loss of MicroRNA-192 promotes fibrogenesis in diabetic nephropathy. *J Am Soc Nephrol*. 2010;21(3):438-447.
45. Ai J, Zhang R, Li Y, et al. Circulating microRNA-1 as a potential novel biomarker for acute myocardial infarction. *Biochem Biophys Res Commun*. 2010;391(1):73-77.
46. Yuan J, Benway CJ, Bagley J, Iacomini J. MicroRNA-494 promotes cyclosporine-induced nephrotoxicity and epithelial to mesenchymal transition by inhibiting PTEN. *Am J Transplant*. 2015;15(6):1682-1691.
47. Andoh TF, Lam TT, Lindsley J, Alpers CE, Benneti WM. Enhancement of chronic cyclosporine nephrotoxicity by sodium depletion in an experimental mouse model. *Nephrology*. 1997;3(6):471-478.
48. Yang CW, Faulkner GR, Wahba IM, et al. Expression of apoptosis-related genes in chronic cyclosporine nephrotoxicity in mice. *Am J Transplant*. 2002;2(5):391-399.
49. Hafner M, Renwick N, Farazi TA, Mihailovic A, Pena JT, Tuschl T. Barcoded cDNA library preparation for small RNA profiling by next-generation sequencing. *Methods*. 2012;58(2):164-170.
50. Hafner M, Landthaler M, Burger L, et al. Transcriptome-wide identification of RNA-binding protein and microRNA target sites by PAR-CLIP. *Cell*. 2010;141(1):129-141.
51. Livak KJ, Schmittgen TD. Analysis of relative gene expression data using real-time quantitative PCR and the 2(-Delta Delta C(T)) Method. *Methods*. 2001;25(4):402-408.
52. Friedlander MR, Mackowiak SD, Li N, Chen W, Rajewsky N. miRDeep2 accurately identifies known and hundreds of novel microRNA genes in seven animal clades. *Nucleic Acids Res*. 2012;40(1):37-52.
53. Mazieres J, Catherinne C, Delfour O, et al. Alternative processing of the U2 small nuclear RNA produces a 19-22nt fragment with relevance for the detection of non-small cell lung cancer in human serum. *PLoS ONE*. 2013;8(3):e60134.
54. Matylla-Kulinska K, Tafer H, Weiss A, Schroeder R. Functional repeat-derived RNAs often originate from retrotransposon-propagated ncRNAs. *Wiley Interdiscip Rev RNA*. 2014;5(5):591-600.

55. Grimson A, Farh KK, Johnston WK, Garrett-Engele P, Lim LP, Bartel DP. MicroRNA targeting specificity in mammals: determinants beyond seed pairing. *Mol Cell*. 2007;27(1):91-105.
56. Bruna A, Nicolas M, Munoz A, Kyriakis JM, Caelles C. Glucocorticoid receptor-JNK interaction mediates inhibition of the JNK pathway by glucocorticoids. *EMBO J*. 2003;22(22):6035-6044.
57. Matsuda S, Shibasaki F, Takehana K, Mori H, Nishida E, Koyasu S. Two distinct action mechanisms of immunophilin-ligand complexes for the blockade of T-cell activation. *EMBO Rep*. 2000;1(5):428-434.
58. Derfoul A, Robertson NM, Hall DJ, Litwack G. The N-terminal domain of the mineralocorticoid receptor modulates both mineralocorticoid receptor- and glucocorticoid receptor-mediated transactivation from Na/K ATPase beta1 target gene promoter. *Endocrine*. 2000;13(3):287-295.
59. Kirschke E, Goswami D, Southworth D, Griffin PR, Agard DA. Glucocorticoid receptor function regulated by coordinated action of the Hsp90 and Hsp70 chaperone cycles. *Cell*. 2014;157(7):1685-1697.
60. Pham TT, Angus SP, Johnson GL. MAP3K1: genomic alterations in cancer and function in promoting cell survival or apoptosis. *Genes Cancer*. 2013;4(11–12):419-426.
61. Chen J, Zmijewska A, Zhi D, Mannon RB. Cyclosporine-mediated allograft fibrosis is associated with micro-RNA-21 through AKT signaling. *Transpl Int*. 2015;28(2):232-245.
62. Git A, Dvinge H, Salmon-Divon M, et al. Systematic comparison of microarray profiling, real-time PCR, and next-generation sequencing technologies for measuring differential microRNA expression. *RNA*. 2010;16(5):991-1006.
63. Pritchard CC, Cheng HH, Tewari M. MicroRNA profiling: approaches and considerations. *Nat Rev Genet*. 2012;13(5):358-369.
64. Krell J, Stebbing J, Carissimi C, et al. TP53 regulates miRNA association with AGO2 to remodel the miRNA-mRNA interaction network. *Genome Res*. 2016;26(3):331-341.
65. Salomon William E, Jolly Samson M, Moore Melissa J, Zamore Phillip D, Serebrov V. Single-molecule imaging reveals that argonaute reshapes the binding properties of its nucleic acid guides. *Cell*. 2015;162(1):84-95.
66. Yoo JK, Jung HY, Kim C-H, Son WS, Kim JK. miR-7641 modulates the expression of CXCL1 during endothelial differentiation derived from human embryonic stem cells. *Arch Pharm Res*. 2013;36(3):353-358.
67. Lee YI, Kwon YJ, Joo CK. Integrin-linked kinase function is required for transforming growth factor beta-mediated epithelial to mesenchymal transition. *Biochem Biophys Res Commun*. 2004;316(4):997-1001.
68. Böttinger EP, Bitzer M. TGF-ß signaling in renal disease. *J Am Soc Nephrol*. 2002;13(10):2600-2610.
69. Matsuda S, Koyasu S. Mechanisms of action of cyclosporine. *Immunopharmacology*. 2000;47(2–3):119-125.
70. Gooch JL, King C, Francis CE, Garcia PS, Bai Y. Cyclosporine A alters expression of renal microRNAs: New insights into calcineurin inhibitor nephrotoxicity. *PLoS ONE*. 2017;12(4):e0175242.

SUPPORTING INFORMATION

Additional Supporting Information may be found online in the supporting information tab for this article.

How to cite this article: Benway CJ, Iacomini J. Defining a microRNA-mRNA interaction map for calcineurin inhibitor induced nephrotoxicity. *Am J Transplant*. 2018;18:796–809. https://doi.org/10.1111/ajt.14503